Enhancing Misalignment Tolerance in Hybrid Wireless Power Transfer System With Integrated Coupler via Frequency Tuning

Fengxian Wang, Qingxin Yang, Xian Zhang, Ting Chen, *Member, IEEE*, and Guangyao Li

***Abstract*—To enhance the misalignment tolerance and system integration of the wireless power transfer (WPT) system, an integrated coupler consisting of capacitors and coils overlapped coaxially is proposed in this article and integrated into the hybrid WPT (HWPT) system without extra compensation components. The system utilizes the complementary characteristics of different transmission channels to realize the synergistic transfer of different coupled powers under a wide coupling range. Based on the mutual influence between capacitors and coils in terms of electrical parameters in a limited axial projection area and the zero-phase-angle condition considering the mutual capacitance obtained by the fundamental harmonics approximation method, the method of regulating the transfer ratio of the two types of coupled powers is mastered. A method to realize the HWPT with high misalignment tolerance characteristics by frequency tracking is proposed to solve the problem of the system's resonant state being disrupted when the position of the integrated coupler is misaligned. The field-circuit coupling model verifies the feasibility of the analysis and transfer method. Finally, an experimental verification platform for 500 W is built to achieve 82.7% power transfer in the WPT system with 40% unidirectional misalignment.**

***Index Terms*—Constant current (CC), high misalignment tolerance, hybrid wireless power transfer (HWPT), integrated coupler, zero-phase-angle (ZPA).**

Manuscript received 10 March 2024; revised 24 April 2024; accepted 8 June 2024. Date of publication 20 June 2024; date of current version 16 July 2024. This work was supported in part by the National Natural Science Foundation of China under Project 52122701 and Project 52307009, in part by the Key Program of Natural Science Foundation of Tianjin under Grant 22JCZDJC00620, in part by the Hebei Provincial Central Guidance Local Science and Technology Development Project 236Z5201G, in part by the Colleges and Universities in Hebei Province Science and Technology Research Project under Grant CXY2024010, in part by the Interdisciplinary Postgraduate Training Program of Hebei University of Technology under Grant HEBUT-Y-XKJC-2022109, in part by the State Key Laboratory of Reliability and Intelligence of Electrical Equipment under Grant EERI_OY2023001, and in part by the S&T Program of Hebei under Grant 225676163GH. Recommended for publication by Associate Editor A. Safaee. *(Corresponding authors: Qingxin Yang; Xian Zhang.)*

Fengxian Wang, Xian Zhang, Ting Chen, and Guangyao Li are with the State Key Laboratory of Reliability and Intelligence of Electrical Equipment, Hebei University of Technology, Tianjin 300401, China, and also with the Hebei Key Laboratory of Equipment and Technology Demonstration of Flexible DC Transmission, Hebei University of Technology, Tianjin 300401, China (e-mail: fx-wang@outlook.com; zhangxian@hebut.edu.cn; tingchen@hebut.edu.cn; lgymecury@163.com).

Qingxin Yang is with the Tianjin University of Technology, Tianjin 300384, China (e-mail: qxyang@tjut.edu.cn).

Color versions of one or more figures in this article are available at https://doi.org/10.1109/TPEL.2024.3416172.

Digital Object Identifier 10.1109/TPEL.2024.3416172

I. Introduction

WIRELESS power transfer (WPT) is an emerging technology that employs spatial electromagnetic transformation to achieve contactless power transfer [1], [2]. This technology addresses the limitations of traditional contact-based power transfer and has garnered increasing attention from researchers and manufacturers due to its flexibility, convenience, and broad applicability. Moreover, the WPT has been progressing towards high-frequency and high-power applications [3]. Due to limitations imposed by transfer power and system efficiency, the large-scale implementations of the WPT technology primarily rely on the near-field effect of the electromagnetic field (EMF) [4].

According to the power transmission channels, WPT technology utilizing the near-field effect of the EMF can be categorized into two types: WPT technology with electric field coupling and WPT technology with magnetic field coupling. Capacitive power transfer (CPT) is a representative example of electric field coupling WPT technology [5], [6], whereas inductive power transfer (IPT) represents magnetic field coupling WPT technology [7], [8], [9]. The two types of power transmission channels possess distinct characteristics. For instance, the electric field coupling transmission channel enables power to be transmitted through metal barriers without significant power losses. However, its widespread adoption has been limited by its constrained transfer distance. On the other hand, the magnetic field coupling transmission channel exhibits a wide transfer range within the near-field EMF environment. Nevertheless, it introduces eddy current losses in the metal within the coupling space, which poses a potential risk to the system's safe operation. Consequently, the two types of power transmission channels possess unique attributes and complement each other [10], [11].

Researchers have increasingly employed multiple types of power transmission channels to address the limitations of the single coupling transmission channel. Lu et al. [12], [13] introduced a novel coupler structure consisting of vertically arranged long metal sheets. This arrangement transfers power simultaneously through the electric field and magnetic field coupling transmission channels. However, this approach increases the system's cost, size, and weight. Luo et al. [14] analyzed the contribution of the two types of transmission channels to power transfer within the SS-type compensation topology. However, this research used separated couplers, which made the system

oversized. To mitigate the challenge, Luo et al. [15] proposed a compact hybrid coupler. However, the research ignores the metal materials' disruption of the system's constant output condition. Besides, the above-mentioned research works all require extra compensation components.

The extra compensation components lead to the complexity of the actual circuit connections and cause system redundancy. To solve this problem, topology integration research is currently a prominent area of research in WPT technology. Yuan et al. [16] proposed a WPT system based on a combined dual-coupled *LCC*-S topology with a transmitter consisting of two mutually decoupled transmitting coils. The design of this structure ensures that the two mutual inductances between the transmitter and receiver exhibit opposite trends in the case of misalignment, thereby enhancing the system's tolerance to high misalignment. Similarly, Dai and Wang [17] introduced a WPT system based on a hybrid topology. This system uses a multilayer self-decoupled compact coil for noncontact power transfer under dual-frequency conditions. The system uses the simultaneous resonance of the fundamental and third harmonic frequencies as a constraint, which effectively reduces the inverter requirements while improving the tolerance of lateral misalignment. To achieve the integrated multiplexing of various functions, the current research on topology integration of WPT mainly concentrated on integrating coils with compensation topologies. The above-mentioned research works still require extra compensation capacitance.

As analyzed, the system integration (size, weight, and circuit connection) needs to be improved in the hybrid WPT (HWPT) system design to fully utilize the potential benefits of multiple power transmission channels [18], [19], [20], [21]. The problem can be solved by combining topology integration. Therefore, this article proposes an HWPT system with a novel integrated coupler consisting of a capacitor and a coil overlap in a coaxial arrangement. It is noteworthy that the capacitor consists of two aluminum metal plates placed vertically. The integrated coupler utilizes the respective characteristics of the two types of materials as the two types of power transmission channels. It is integrated into the system, which has the distinctive merit that no extra compensating components are required. It should be noted that the integration method proposed in this article differs from conventional topology integration, in which only coils are integrated into the system. This article integrates both coils and capacitors into the main circuit.

The proposed HWPT system has several advantages, which are outlined as follows.

1) *Enhancing misalignment tolerance:* The system realizes coupled power transfer by using the capacitor and the coil as electric field and magnetic field coupling transmission channels, respectively. The synergistic transfer of coupled powers is realized under broad coupling range conditions by leveraging the complementary characteristics of the two types of power transmission channels.
2) *Enhancing system integration:* The coupler is integrated into the system's compensation topology without extra compensation components. This integration facilitates the multiplexing of power transfer and circuit compensation and improves the system's overall performance.
3) *Enhancing Electrical Shielding:* Due to the aluminum metal plates, the integrated coupler provides better electrical shielding and minimizes the risk of EMF leakage. Using lightweight aluminum metal plates reduces the coupler's overall weight compared with soft magnetic materials.

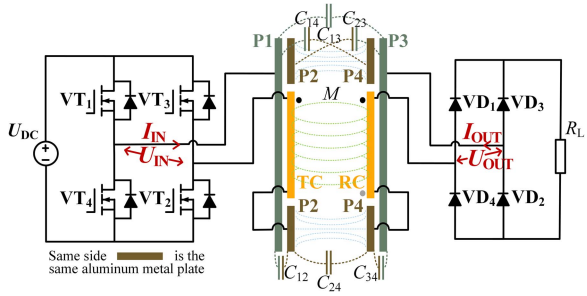

Fig. 1. Main topology of the proposed HWPT system.

The rest of this article is organized as follows. Section II introduces the integrated coupler's structure and analyzes the influence of the geometric parameters on the inductance and capacitance. In addition, it analyzes the HWPT system's power transfer principle and obtains the requirements for zero-phase-angle (ZPA) input and load-independent constant current (CC) output. Section III proposes a transfer method of the HWPT by frequency tracking to address the challenge of system resonance disruption caused by the integrated coupler's misalignment and analyzes the system's misalignment characteristics. Section IV offers experimental results to validate the effectiveness of the proposed transfer method. Finally, Section V concludes this article, summarizing the essential findings and contributions of the research.

This article proposes a new HWPT method that compensates for the decrease in electromagnetic power due to the positional misalignment of the system under the single coupling form by the synergistic transfer of the two types of coupled powers. The experimental results show that the HWPT system is tolerant to misalignment. The work in this article will inform the further development of HWPT and perfect the HWPT technique in terms of misalignment.

II. HWPT System

A. Proposed HWPT System

In this article, the system architecture of the proposed HWPT system is shown in Fig. 1. The main circuit is composed of the dc power supply, high-frequency full-bridge inverter formed by VT_1-VT_4, integrated coupler, rectifier, and the load resistance R_L. The novel integrated coupler integrated into the main circuit consists of a capacitor and a coil overlap in a coaxial arrangement. It is noteworthy that the capacitor is constructed with two vertically oriented aluminum metal plates. P1 and P2 represent the two aluminum metal plates constituting the capacitor in the

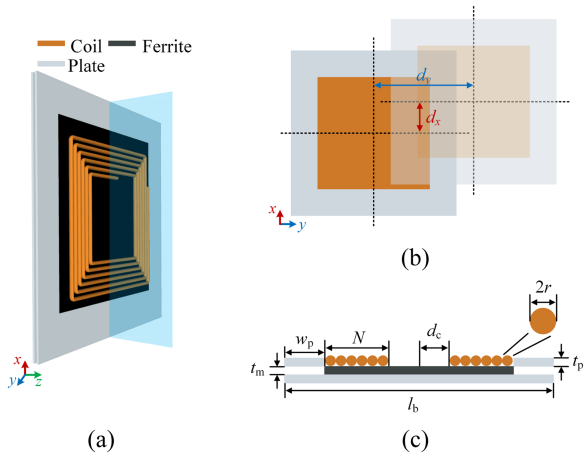

Fig. 2. Structure and dimension of the integrated coupler. (a) Three-dimensional view. (b) Misalignment in the x-direction and y-direction. (c) Longitudinal section.

primary side integrated coupler. In comparison, P3 and P4 represent the two aluminum metal plates constituting the capacitor in the secondary side integrated coupler. The aluminum metal plates (P1–P4) with identical color markings on the same side represent a single aluminum plate. In this case, the main circuit has no extra compensation components. As shown in Fig. 1, there is magnetic field coupling between the integrated couplers, where M represents the mutual inductance.

The proposed HWPT system's topology resembles the traditional SS-type topology used in the IPT system. The key distinction lies in the coupling between the capacitors, which enables electromagnetic power transfer from the primary to the secondary side through the system's electric field.

B. Integrated Coupler

The integrated coupler is crucial in transferring coupled power through EMF. Fig. 2(a) shows the proposed integrated coupler in which the capacitor and coil overlap in a coaxial arrangement. To mitigate the eddy current effects caused by the coil on the capacitor, which is constructed with aluminum metal plates, the ferrite is introduced to separate the coil from the capacitor. This structure minimizes the adverse impact of eddy currents and enhances the coil's quality factor. The integrated coupler's longitudinal section is shown in Fig. 2(c) to demonstrate the integrated coupler structure visually. In the proposed integrated coupler, the central portion consists of an aluminum metal plate, a ferrite, and a coil when moving from the transfer space's outer area to the transfer space's inner area. Meanwhile, the outer portion consists of an aluminum metal plate and another aluminum metal plate. The ferrite dimensions in x- and y-axis match the coil. In Fig. 2(c), t_{m} denotes the gap between the metal plates, t_{p} denotes the thickness of the metal plates, N denotes the coil's turn, and r denotes the coil's wire radius. The back aluminum metal plate's length is denoted by the l_{b}. Meanwhile, d_{c} denotes the coil's inner diameter, w_{p} denotes the abdominal aluminum metal plate's width, and d denotes the

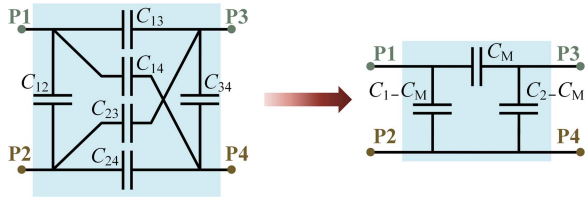

Fig. 3. Circuit model of the capacitors.

distance between the integrated couplers. t_{f} denotes the thickness of the ferrite.

The circuit model of the capacitors is shown in Fig. 3. According to Zhang et al. [22], the six-capacitor model can effectively represent the distributed capacitance parameters of the integrated couplers. In this model, C_{ij} denotes the coupling capacitance between the aluminum metal plates Pi and Pj ($i, j = 1, 2, 3, 4$). The six-capacitor model can be further reduced to a three-capacitor model for simplification and practical implementation. It is a typical two-port network equivalent to the current source model. In this model, C_1 and C_2 denote the self-capacitance, and C_{M} denotes the mutual capacitance. The self-capacitance and mutual capacitance can be expressed as

$$\begin{cases} C_1 = C_{12} + \frac{(C_{13}+C_{14})(C_{23}+C_{24})}{C_{13}+C_{14}+C_{23}+C_{24}} \\ C_2 = C_{34} + \frac{(C_{13}+C_{23})(C_{14}+C_{24})}{C_{13}+C_{14}+C_{23}+C_{24}} \\ C_M = \frac{C_{13}C_{24}-C_{14}C_{23}}{C_{13}+C_{14}+C_{23}+C_{24}} \end{cases}. \tag{1}$$

The distinctive feature of the proposed integrated coupler, as compared to the conventional couplers, is that it consists of not only the coils but also the compensation capacitors. In this configuration, the coils and the compensation capacitors contribute to the magnetic field coupling transmission channel and the electric field coupling transmission channel, respectively. The integrated coupler's electrical characteristics are affected by its structure. It is also affected by the mutual interactions between the coil and the capacitor. Understanding and analyzing these affecting laws are essential for the subsequent design of the integrated coupler. The coil's turn and the gap between the metal plates are the adjustment objects to streamline the design process.

Fig. 4 shows the influence of metal components on the integrated coupler's electrical parameters within a limited area. This area is determined by the axial projection of the aluminum metal plate and the coil. The integrated coupler's dimensions are $l_{\mathrm{b}} = 300$ mm, $r = 1$ mm, $d_{\mathrm{c}} = 20$ mm, and $d = 10$ mm. The relative position of the coil and the metal plate does not change with t_{m}. The coil is at the center of the integrated coupler, with the ferrite close to the bigger metal plate (P1/P3). In this case, there is no openings are required in the metal plates P1 and P3, and the gap between the metal plates does not affect the position of the coil and the ferrite. Table I shows the design values of the integrated coupler. The abdominal aluminum metal plate's width and the coil's turns meet $l_{\mathrm{b}} = 2(d_{\mathrm{c}} + w_{\mathrm{p}} + 2rN)$. Therefore, when N is adjusted, w_{p} is changed.

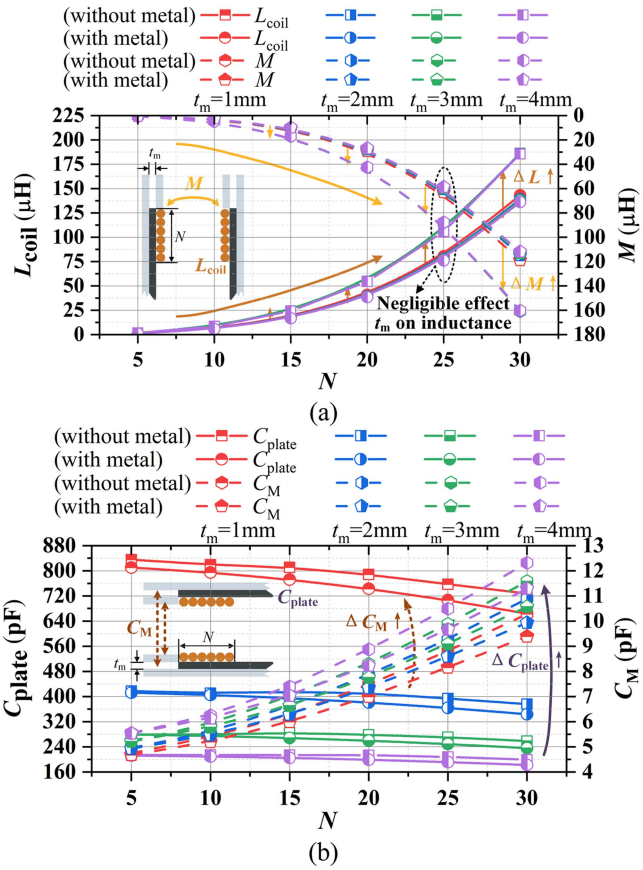

Fig. 4. Effect of metals on the electrical parameters of the integrated coupler. (a) Inductance. (b) Capacitance.

TABLE I
SIMULATION PARAMETERS

Parameter	Design value	Note
l_b	300 mm	Metal plate's length
t_p	2 mm	Metal plate's thickness
t_f	2 mm	Ferrite's thickness
r	1 mm	Coil's wire radius
d_c	10 mm	Coil's inner diameter
d	10 mm	Transmission distance

The metal components affect the integrated coupler's electrical parameters, especially the inductance. In this case, the integrated coupler's inductance decreases due to the influence of the metal components, as shown in Fig. 4(a). For the integrated coupler's inductance, without metal means no metal plate. The integrated coupler's self-inductance and mutual inductance increase as the coil's turn increases. While metal components may decrease the integrated coupler's overall inductance, the coil's turn is the primary factor driving the integrated coupler's inductance variations. The ferrite separates the coils from the metal plates P1 and P3. The influence of the metal plates P1 and P3 on the integrated coupler's inductance is suppressed. Meanwhile, the position and size of the metal plates P2 and P4 do not change with the gap between capacitor plates, which does not affect the integrated coupler's inductance. Therefore, the gap between capacitor plates does not affect the integrated coupler's inductance.

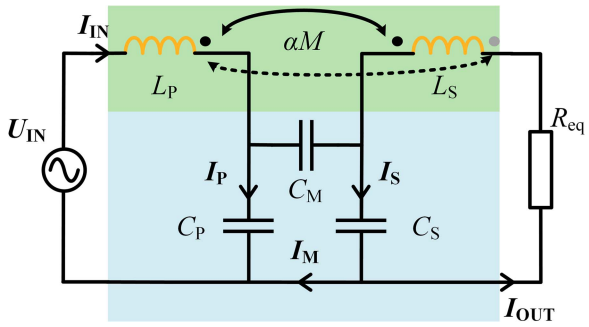

Fig. 5. Equivalent circuit of the proposed HWPT system under the fundamental component.

The coil's turn and the gap between the metal plates affect the integrated coupler's capacitance, as shown in Fig. 4(b). For the integrated coupler's capacitance, without metal means no coil. It should be noted that changing the coil's turn with or without metal conditions changes the plate's width w_p. Fig. 4(b) shows that the integrated coupler's capacitance varies with the coil's turn, due to the corresponding changes in the plate's width. The integrated coupler's self-capacitance decreases as the coil's turn increases (the plate's width decreases). This is caused by the decreases in C_{12} and C_{34} due to the decreased effective positive area between the same side aluminum metal plates. Instead, the integrated coupler's mutual capacitance increases as the coil's turn increases (the plate's width decreases). This is caused by the decreases in C_{14} and C_{23} due to the decreased effective positive area between the opposite side aluminum metal plates. The gap between the metal plates similarly affects the integrated coupler's capacitance as the coil's turn (the plate's width). The integrated coupler's self-capacitance decreases as the gap between the metal plates increases. Instead, the integrated coupler's mutual capacitance increases as the gap between the metal plates increases.

The impact of metal components on the integrated coupler can be better understood by analyzing the integrated coupler's electrical parameters under different the coil's turn and the gap between the metal plates. It is essential to note that the integrated coupler's inductance is primarily affected by the coil's turn, and the integrated coupler's capacitance is simultaneously determined by the coil's turns (plate's width) and the gap between the metal plates. The discussion in this section will provide the basis for the subsequent analysis in Section III-B on the system's misalignment characteristics.

C. Circuit Working Principle

Fig. 5 shows the equivalent circuit of the proposed HWPT system. The working principle of the proposed HWPT system is analyzed using the fundamental harmonics approximation method. In Fig. 5, $\boldsymbol{U}_{\mathbf{IN}}$ denotes the input voltage, R_{eq} denotes the equivalent load, and M denotes the mutual inductance between the coils. Meanwhile, $C_P = C_1 - C_M$, $C_S = C_2 - C_M$.

The system can be modeled as

$$\begin{cases} \frac{1}{\mathrm{j}\omega \mathbf{C_P}}\mathbf{I_P} + \mathrm{j}\omega L_\mathbf{P}\mathbf{I_{IN}} + \mathrm{j}\omega\alpha M\mathbf{I_{OUT}} = \mathbf{U_{IN}} \\ \frac{1}{\mathrm{j}\omega \mathbf{C_M}}\mathbf{I_M} + \frac{1}{\mathrm{j}\omega \mathbf{C_S}}\mathbf{I_S} = \frac{1}{\mathrm{j}\omega \mathbf{C_P}}\mathbf{I_P} \\ \mathrm{j}\omega L_\mathbf{S}\mathbf{I_{OUT}} + \mathrm{j}\omega\alpha M\mathbf{I_{IN}} + R_\mathbf{eq}\mathbf{I_{OUT}} = -\frac{1}{\mathrm{j}\omega \mathbf{C_S}}\mathbf{I_S} \\ \mathbf{I_P} + \mathbf{I_M} = \mathbf{I_{IN}} \\ \mathbf{I_{OUT}} + \mathbf{I_M} = \mathbf{I_S} \end{cases} \tag{2}$$

where L_P and L_S denote the transmitting coil's self-inductance and the receiving coil's self-inductance, respectively. α denotes the connection of the coils, $\alpha = 1$ when coils are connected in phase, and $\alpha = -1$ when coils are connected out of phase.

The system's output current can be expressed as

$$\begin{cases} \mathbf{I_{out}} = \frac{\mathbf{jX_4U_{IN}}}{1-X_1-\mathbf{j}X_3R_\mathbf{L}} \\ X_\mathbf{plate} = \omega^2\left[C_\mathbf{M}\left(C_\mathbf{P}+C_\mathbf{S}\right)+C_\mathbf{P}C_\mathbf{S}\right] \\ X_1 = \omega^2\left(X_2 + X_5X_\mathbf{plate} - 2\alpha MC_\mathbf{M}\right) \\ X_2 = L_\mathbf{P}\left(C_\mathbf{M}+C_\mathbf{P}\right)+L_\mathbf{S}\left(C_\mathbf{M}+C_\mathbf{S}\right) \\ X_3 = \omega\left(L_\mathbf{P}X_\mathbf{plate} - C_\mathbf{M} - C_\mathbf{S}\right) \\ X_4 = \omega\left(\alpha MX_\mathbf{plate} - C_\mathbf{M}\right) \\ X_5 = M^2 - L_\mathbf{P}L_\mathbf{S} \end{cases}. \tag{3}$$

To realize the system's CC output, it is necessary to satisfy

$$X_\mathbf{3} = 0 \Rightarrow L_\mathbf{P} = \frac{C_\mathbf{M}+C_\mathbf{S}}{X_\mathbf{plate}}. \tag{4}$$

Due to the symmetry topology, it assumed that

$$\begin{cases} L_\mathbf{P} = \frac{C_\mathbf{M}+C_\mathbf{S}}{X_\mathbf{plate}} \\ L_\mathrm{S} = \frac{C_\mathbf{M}+C_\mathbf{P}}{X_\mathbf{plate}} \end{cases}. \tag{5}$$

The system's input current can be expressed as

$$\mathbf{I_{IN}} = \frac{\mathbf{U_{IN}}R_\mathbf{eq}X_\mathbf{plate}^2}{X_\mathbf{5}^2}. \tag{6}$$

The system's input impedance can be expressed as

$$Z_\mathbf{IN} = \frac{\mathbf{U_{IN}}}{\mathbf{I_{IN}}} = \frac{X_\mathbf{5}^2}{R_\mathbf{eq}X_\mathbf{plate}^2}. \tag{7}$$

At this point, Im(ZIN) = 0. The imaginary part of the system's input impedance is zero, and the system satisfies the ZPA condition. Then, the system's output current can be expressed as

$$\mathbf{I_{OUT}} = -\frac{\mathrm{j}\mathbf{U_{IN}}X_\mathbf{plate}}{X_5}. \tag{8}$$

At this point, the output current is independent of the equivalent load. The system is made to satisfy the ZPA input and CC output in (5).

The current flowing through the mutual capacitance can be expressed as

$$\mathbf{I_M} = \frac{\omega C_\mathbf{M}\left[\omega C_\mathbf{S}R_\mathbf{eq}X_\mathbf{plate} + \mathrm{j}\omega^2 C_\mathbf{P}X_5\right]\mathbf{U_{IN}}}{X_\mathbf{5}^2}. \tag{9}$$

The coupled power transmitted through the HWPT system's magnetic field can be expressed as

$$\begin{aligned} P_\mathbf{M} &= \mathrm{Re}\left[\mathrm{j}\omega M\mathbf{I_{IN}}(-\mathbf{I_{OUT}})^*\right] \\ &= \frac{\omega\alpha MX_\mathbf{plate}^3}{\left(\omega\alpha MX_\mathbf{plate} - \omega C_\mathbf{M}\right)^3}\mathbf{U_{IN}^2}\mathbf{R_{eq}}. \end{aligned} \tag{10}$$

The coupled power transmitted through the HWPT system's electric field can be expressed as

$$\begin{aligned} P_\mathbf{E} &= \mathrm{Re}\left\{\left[\mathbf{U_{IN}} - \mathrm{j}\omega\left(L_\mathbf{P}\mathbf{I_{IN}} + M\mathbf{I_{OUT}}\right)\right]\mathbf{I_M^*}\right\} \\ &= -\frac{\omega C_\mathbf{M}X_\mathbf{plate}^2}{\left(\omega\alpha MX_\mathbf{plate} - \omega C_\mathbf{M}\right)^3}\mathbf{U_{IN}^2}\mathbf{R_{eq}}. \end{aligned} \tag{11}$$

The ratio between the two types of coupled powers can be expressed as

$$\beta = \frac{P_\mathbf{E}}{P_\mathbf{M}} = -\frac{C_\mathbf{M}}{\alpha X_\mathbf{plate}M}. \tag{12}$$

When the coils are connected in phase ($\alpha = 1$), $\beta < 0$ means that the coupled power transmitted through the electric field and the coupled power transmitted through the magnetic field are transmitted in opposite directions. In other words, P_M is transferred from the primary side to the secondary side, while P_E is transferred from the secondary side to the primary side. On the other hand, when the coils are connected out of phase ($\alpha = -1$), $\beta > 0$ means that the coupled power transmitted through the electric field and the coupled power transmitted through the magnetic field are transmitted in the same directions. The coils' connection is essential to leverage the integrated coupler for effective power transfer. The choice of coils' connection mode is discussed in Section III-B.

III. Coupled Power Transfer Method

A. Tracking Frequency

From the discussion in Section II-C, it is evident that (5) must be satisfied to ensure the optimal resonance state of the HWPT system. However, according to the discussion in Section II-B, the integrated coupler's electrical parameters can change when the position of the integrated coupler is misaligned. As a result, the resonance state is disrupted. This article proposes a transfer method to realize the HWPT with high misalignment tolerance characteristics by frequency tracking in such cases. This transfer method compensates for the change in the integrated coupler's electrical parameters owing to misalignment by adjusting the system's working frequency. It allows the special equation previously described to hold for any state of misalignment.

To simplify the analysis, it is assumed that the secondary side coupler is symmetrical with the primary side coupler and satisfies $L_\mathrm{P} = L_\mathrm{S} = L_\mathrm{coil}$ and $C_1 = C_2 = C_\mathrm{plate}$. To express the level of coupling of EMFs, define the electric field coupling coefficient $k_\mathrm{E} = C_\mathrm{M}/C_\mathrm{plate}$ and magnetic field coupling coefficient $k_\mathrm{M} = M/L_\mathrm{coil}$. From (5), the working frequency in any state of misalignment needs to satisfy

$$\omega_\mathbf{r} = \frac{1}{\sqrt{\left(1-k_E^2\right)C_\mathbf{plate}L_\mathbf{coil}}}. \tag{13}$$

At this point, the HWPT system is ensured to be resonant under any coupling condition at best. Bringing (13) into (10) and (11), the coupled power transmitted through the HWPT system's

magnetic field under tracking ω_{r} can be expressed as

$$P_{\mathbf{M}-\omega_{\mathrm{r}}}=-\frac{\alpha C_{\mathbf{plate}} k_{\mathbf{M}}\left(1-k_{\mathbf{E}}^{2}\right)}{L_{\mathbf{coil}}\left(k_{\mathbf{E}}-\alpha k_{\mathbf{M}}\right)^{3}}\mathbf{U}_{\mathbf{IN}}^{2}R_{\mathbf{eq}}. \tag{14}$$

The coupled power transmitted through the HWPT system's electric field under tracking ω_{r} can be expressed as

$$P_{\mathbf{E}-\omega_{\mathrm{r}}}=\frac{k_{\mathbf{E}} C_{\mathbf{plate}}\left(1-k_{\mathbf{E}}^{2}\right)}{L_{\mathbf{coil}}\left(k_{\mathbf{E}}-\alpha k_{\mathbf{M}}\right)^{3}}\mathbf{U}_{\mathbf{IN}}^{2}\mathbf{R}_{\mathbf{eq}}. \tag{15}$$

The ratio of the two types of coupled powers transmitted by the system under tracking ω_{r} can be expressed as

$$\beta_{\omega_{\mathrm{r}}}=-\frac{k_{\mathbf{E}}}{\alpha k_{\mathbf{M}}}. \tag{16}$$

According to (16), the power ratio is related to the system's coupling coefficient. Therefore, a reasonable design of the integrated coupler's structure can adjust the power ratio. Meanwhile, the power ratio fluctuates when the position of the integrated coupler is misaligned due to the system's coupling coefficient fluctuation.

The system's output power can be expressed as

$$P_{\mathbf{HPT}-\omega_{\mathrm{r}}}=P_{\mathbf{M}-\omega_{\mathrm{r}}}+P_{\mathbf{E}-\omega_{\mathrm{r}}}=\frac{C_{\mathbf{plate}}\left(1-k_{\mathbf{E}}^{2}\right)}{L_{\mathbf{coil}}\left(k_{\mathbf{E}}-\alpha k_{\mathbf{M}}\right)^{2}}\mathbf{U}_{\mathbf{IN}}^{2}\mathbf{R}_{\mathbf{eq}}. \tag{17}$$

Assume that the system's reference working frequency is ω_i when the position of the integrated coupler is misaligned. The self-inductance and self-capacitance of the integrated coupler can be expressed in (5) as

$$\begin{cases} L_{\mathbf{coil}}=\frac{1}{\omega_i^2 C_{\mathbf{plate}}\left(1-k_{\mathbf{E}}^{2}\right)} & (\mathrm{a}) \\ C_{\mathbf{plate}}=\frac{1}{\omega_i^2 L_{\mathbf{coil}}\left(1-k_{\mathbf{E}}^{2}\right)} & (\mathrm{b}) \end{cases}. \tag{18}$$

Equation (18) is an equivalent expression of the integrated coupler's electrical parameters when the system satisfies both the resonance condition and the optimum working frequency.

Equation (19a)–(19f), shown at the bottom of this page, is obtained by substituting (18a) into (17), which represents the HWPT system's output power concerning the self-capacitance. Equation (19b) is obtained by substituting (18b) into (17), which represents the HWPT system's output power concerning the self-inductance. When both the IPT and CPT systems use SS-type compensation topology, the working frequency is consistent with the reference working frequency ω_i of the HWPT system.

L_{IPT} denotes the coil self-inductance of the IPT system with symmetrical couplers on both sides, and C_{CPT} denotes the metal plate self-capacitance of the CPT system with symmetrical couplers on both sides. Equation (19c) represents the output power of the IPT system under constant voltage source excitation when $L_{\mathrm{IPT}}=L_{\mathrm{coil}}$. Equation (19d) represents the output power of the CPT system under constant voltage source excitation when $C_{\mathrm{CPT}}=C_{\mathrm{plate}}$. k_{H} denotes the HWPT system's hybrid coupling coefficient. k_{Es} and k_{Ms} denote the coupling coefficient of the single-type coupler (only coils or capacitors).

According to the discussion in Section II-B, the electric field coupling coefficient k_{E} between the integrated coupler's aluminum metal plates and the electric field coupling coefficient k_{Es} between the aluminum metal plates of the same size (without the influence of the coils) satisfy (19e) due to the interaction between the coils and the capacitors. Similarly, the magnetic field coupling coefficient k_{M} between the integrated coupler's coils and the magnetic field coupling coefficient k_{Ms} between the identical-size coils (without the influence of the aluminum metal plate) satisfies (19e).

From (19c) and (19d), it is evident that the output power of the CPT system and the output power of the IPT system are related to the coupling coefficient. When the position of the integrated coupler is misaligned, the output power will fluctuate due to the fluctuation of the coupling coefficient. Smoothing the coupling coefficient's variation curve with the system position can improve the system's tolerance to position misalignment.

Comparing (19a) with (19c), it is evident that to ensure the output characteristics of the HWPT system are better than the IPT system, the hybrid coupling coefficient can be optimized so that its rate of change is lower than that of the k_{Ms}. Similarly, a comparison of (19b) and (19d) shows that optimizing the hybrid coupling coefficient so that its rate of change is lower than that of the k_{Es} can ensure that the output characteristics of the HWPT system outperform the CPT system. The transmission characteristics of the HWPT system are influenced by $k_{\mathrm{H}}=k_{\mathrm{E}}-\alpha k_{\mathrm{M}}$. If $k_{\mathrm{H}}>k_{\mathrm{M}}$ or k_{E}, the WPT system with better output characteristics can be obtained.

B. Transmission Efficiency

This section analyzes the effect of parasitic resistance on transmission efficiency (ac–ac). The power losses of the integrated coupler of the HWPT system consist of the coil losses and the capacitor losses. R_{LP} and R_{LS} denote the resistance of the primary coil and the resistance of the secondary coil, respectively. G_{CP} and G_{CS} denote the conductance of the primary capacitor and the conductance of the secondary capacitor, respectively. The transmission efficiency can be expressed as

$$\eta=\frac{P_{OUT}}{P_{OUT}+I_{\mathbf{IN}}^{2}R_{\mathbf{LP}}+I_{\mathbf{OUT}}^{2}R_{\mathbf{LS}}+U_{\mathbf{CP}}^{2}G_{\mathbf{CP}}+U_{\mathbf{CS}}^{2}G_{\mathbf{CS}}} \tag{20}$$

$$\begin{cases} P_{\mathbf{HPT-L}}=\frac{1}{\omega_i^2 L_{\mathbf{coil}}^2\left(k_{\mathbf{E}}-\alpha k_{\mathbf{M}}\right)^2}\mathbf{U}_{\mathbf{IN}}^{2}\mathbf{R}_{\mathbf{eq}}=\frac{1}{\omega_{\mathbf{i}}^{2}\mathbf{L}_{\mathbf{coil}}^{2}\mathbf{k}_{\mathbf{H}}^{2}}\mathbf{U}_{\mathbf{IN}}^{2}\mathbf{R}_{\mathbf{eq}} & (\mathbf{a}) \\ P_{\mathbf{HPT-C}}=\frac{\omega_i^2 C_{\mathbf{plate}}^2\left(1-k_{\mathbf{E}}^{2}\right)^2}{\left(k_{\mathbf{E}}-\alpha k_{\mathbf{M}}\right)^2}\mathbf{U}_{\mathbf{IN}}^{2}\mathbf{R}_{\mathbf{eq}}\approx\frac{\omega_{\mathbf{i}}^{2}\mathbf{C}_{\mathbf{plate}}^{2}}{\mathbf{k}_{\mathbf{H}}^{2}}\mathbf{U}_{\mathbf{IN}}^{2}\mathbf{R}_{\mathbf{eq}} & (\mathbf{b}) \end{cases}$$

$$\begin{cases} P_{\mathbf{IPT}}=\frac{1}{\omega_i^2 L_{\mathbf{coil}}^2 k_{\mathbf{Ms}}^2}\mathbf{U}_{\mathbf{IN}}^{2}\mathbf{R}_{\mathbf{eq}} & (\mathbf{c}) \\ P_{\mathbf{CPT}}=\frac{\omega_i^2 C_{\mathbf{plate}}^2\left(k_{\mathbf{Es}}^{2}-1\right)^2}{k_{\mathbf{Es}}^{2}}\mathbf{U}_{\mathbf{IN}}^{2}\mathbf{R}_{\mathbf{eq}}\approx\frac{\omega_{\mathbf{i}}^{2}\mathbf{C}_{\mathbf{plate}}^{2}}{\mathbf{k}_{\mathbf{Es}}^{2}}\mathbf{U}_{\mathbf{IN}}^{2}\mathbf{R}_{\mathbf{eq}} & (\mathbf{d}) \\ k_{\mathbf{E}}\le k_{\mathbf{Es}}, k_{\mathbf{M}}\le k_{\mathbf{Ms}} & (e) \\ k_{\mathbf{H}}=k_{\mathbf{E}}-\alpha k_{\mathbf{M}} & (f) \end{cases} \tag{19}$$

where U_{CP} and U_{CS} denote the primary capacitor's terminal voltage and the secondary capacitor's terminal voltage, respectively.

Assuming that the coupler is symmetric, $R_{LP} = R_{LS} = R_{coil}$, and $G_{CP} = G_{CS} = G_{plate}$. Substituting $P_{OUT} = P_E + P_M = (1+\beta)P_M$ into (20), the transmission efficiency can be further expressed as

$$\eta = \frac{(1+\beta)}{(1+\beta)+\frac{1}{k_M Q_L}\left(\frac{1}{G_I}+G_I\right)+\frac{\beta}{k_E Q_C}\left(\frac{1}{G_U}+G_U\right)} = \frac{1}{1+\frac{1}{k_M Q_L \xi_I(1+\beta)}+\frac{\beta}{k_E Q_C \xi_U(1+\beta)}} \tag{21}$$

where $Q_L = \omega L_{coil}/R_{coil}$ denotes the coils' quality factor. $Q_C = \omega C_{plate}/G_{plate}$ denotes the capacitors' quality factor. $G_I = I_{IN}/I_{OUT}$ and $G_U = U_{CS}/U_{CP}$. $\xi_I = G_I/(1+G2\,\mathrm{I})$ and $\xi_U = G_U/(1+G2\,\mathrm{U})$.

Substituting (16) into (21), the system transmission efficiency under tracking ω_r can be expressed as

$$\eta_{HWPT} = \frac{1}{1+\frac{1}{k_H Q_C \xi_U}-\frac{1}{\alpha k_H Q_L \xi_I}}. \tag{22}$$

According to (22), the transmission efficiency is affected by the coils' quality factor, the capacitors' quality factor, and the two types of coupling coefficients.

Comparing the transmission efficiency of the HWPT system proposed in this article with that of the single coupling WPT system. Assuming $\beta = 0$, the IPT system's transmission efficiency can be expressed as

$$\eta_{IPT} = \frac{1}{1+\frac{1}{k_{Ms} Q_{Ls} \xi_I}}. \tag{23}$$

Similarly, assuming $\beta = \infty$, the CPT system's transmission efficiency can be expressed as

$$\eta_{CPT} = \frac{1}{1+\frac{1}{k_{Es} Q_{Cs} \xi_U}}. \tag{24}$$

To ensure the transmission efficiency of the HWPT system proposed in this article with that of the single coupling WPT system, the following inequality needs to satisfy

$$\begin{cases} \frac{1}{k_H Q_C \xi_U}-\frac{1}{\alpha k_H Q_L \xi_I} < \frac{1}{k_{Ms} Q_{Ls} \xi_I} \\ \frac{1}{k_H Q_C \xi_U}-\frac{1}{\alpha k_H Q_L \xi_I} < \frac{1}{k_{Es} Q_{Cs} \xi_U} \end{cases} \tag{25}$$

where Q_{Ls} and Q_{Cs} denote the quality factor of the single-type coupler (only coils or capacitors), k_{Es} and k_{Ms} denote the coupling coefficient of the single-type coupler (only coils or capacitors).

The introduction of the metal plates causes a decrease in the coil's quality factor due to the eddy current effect, $Q_L > Q_{Ls}$. Meanwhile, the capacitor's quality factor is considered independent of the coil due to the capacitor's metal-spanning capability, $Q_C \approx Q_{Cs}$. To satisfy inequality (25), it needs to be ensured that the hybrid coupling coefficient is sufficiently optimal to counteract the decrease in the HWPT system's transmission efficiency due to the decrease in the coil's quality factor.

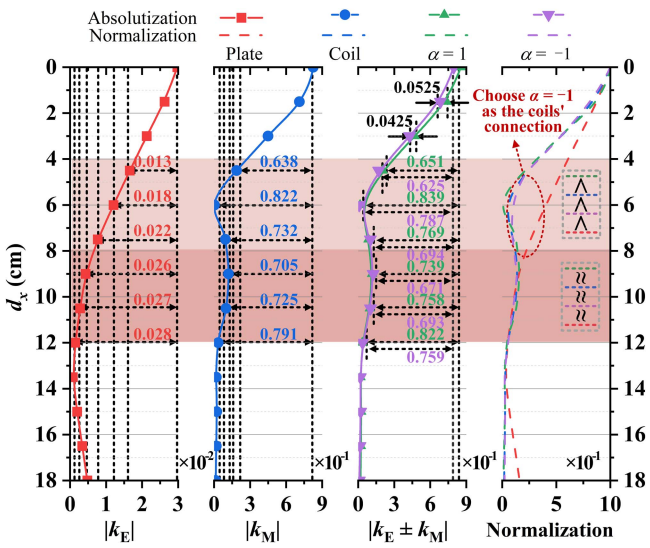

Fig. 6. Variations of coupling coefficient and normalized coupling coefficient with position.

The integrated coupler structure needs to be designed rationally to realize the sizable hybrid coupling coefficient and sizable coil quality factor. This article uses the integrated coupler in which the metal plates and coils overlap in a coaxial arrangement. The area of the metal plates (P2 and P4) close to the coil is limited. The metal plates with the bigger area (P1 and P3) are far away from the coil, and the ferrite binds the magnetic field generated by the coil. Therefore, the coil's quality factor under the influence of the metal plates is still sizable. Meanwhile, the hybrid coupling coefficient of the HWPT system is better than the coupling coefficient of the single coupling WPT system, as shown in the discussion in Section III-A. In summary, the rational design of the integrated coupler is the key to ensuring the HWPT system has high transmission efficiency.

C. System Misalignment Characteristics

The proposed HWPT system based on the integrated coupler realizes the synergistic transfer of two types of coupled powers. In this section, the field-circuit coupling model analyzes the transfer system's misalignment characteristics. Select $N = 30$, $t_m = 2$ mm as the integrated coupler's structure, and the ratio of the two types of coupled powers $\beta = 0.04$. The integrated coupler's self-inductance and self-capacitance are 139 μH and 344 pF, respectively. When the position of the integrated coupler is not misaligned, the integrated coupler's mutual inductance and mutual capacitance are 115 μH and 9.93 pF, respectively. As shown in Fig. 2. (b), d_x and d_y denote the misalignment of the coupler in the x-direction and y-direction, respectively.

Fig. 6 shows the coupling coefficient and normalized coupling coefficient of the three types of WPT systems under different positional misalignments. Using the min-max normalization method to compare different types of coupling coefficients, which satisfies $X_{norm} = (X\text{-}X_{min})/(X_{max}\text{-}X_{min})$, where X ($|k_E|$ || $|k_M|$ || $|k_E \pm k_M|$) denotes different types of absolute coupling coefficients data, X_{min} and X_{max} denote the minimum and

maximum values of all the data in the dataset, respectively, and X_{norm} denotes the normalized data. The magnetic field coupling coefficient and the electric field coupling coefficient decrease when the integrated coupler undergoes displacement. Remarkably, when the position of the integrated coupler is misaligned by 70 mm, the magnetic field coupling coefficient increases slightly, owing to the capacitor's reverse compensation effect. As discussed in Section I regarding the characteristics of the two types of power transmission channels, the rate of decrease in the electric field coupling coefficient is lower than the rate of decrease in the magnetic field coupling coefficient when the position of the integrated coupler is misaligned. In the proposed HWPT system, the hybrid coupling coefficient is a mutual compensation between the magnetic field coupling coefficient and the electric field coupling coefficient. The coils' connection influences the hybrid coupling coefficient, especially within the range of positional misalignment from 40 to 80 mm. When the coils are connected out of phase, the rate of decrease in the hybrid coupling coefficient is between the rate of decrease in the magnetic field coupling coefficient and the electric field coupling coefficient. From (19), it is evident that the reduction of the rate of decrease in the coupling coefficient enhances the system's tolerance to misalignment. As a result of the above-mentioned discussion, the out-of-phase is chosen in this article as the coils' connection. The coupled power transfer through a magnetic field is higher than that through an electric field because the electric field coupling strength is lower than the magnetic field coupling strength. It should be noted that the introduction of the coupled power transfer through the electric field in this article is not to replace the coupled power transfer through the magnetic field completely but rather to compensate for the decrease of the coupled power transfer through the magnetic field due to the positional misalignment.

According to the discussion in Section II-B, it is evident that the integrated coupler's inductance and capacitance will fluctuate as the system undergoes displacement, as shown in Fig. 7. This fluctuation will cause the system's resonant state to be disrupted. However, the prerequisite for the proposed HWPT system to realize the synergistic transfer of two types of coupled powers is that the system is resonant. To solve this problem, this article proposes a coupled power transfer method based on tracking frequency in Section III-C, which adjusts the system's working frequency to satisfy (13). According to the coupled power transfer method proposed in this article, the system's working frequency varies with the positional misalignment to ensure that the system remains in the optimal resonance state, as shown in Fig. 7. For the integrated coupler's dimensions chosen in this article, the optimum working frequency follows a convex function trend (increasing and then decreasing).

The main difference between this article and the existing work is the attention to the problem that the resonant state of the HWPT system is disrupted due to parameters drifting. The system's working frequency is actively adjusted to ensure the optimal operating state of the system at any misalignment position. By achieving maximized synergistic transfer of two types of coupled powers, the misalignment tolerance and integrated output characteristics of the WPT system are enhanced in the case of coupling misalignment.

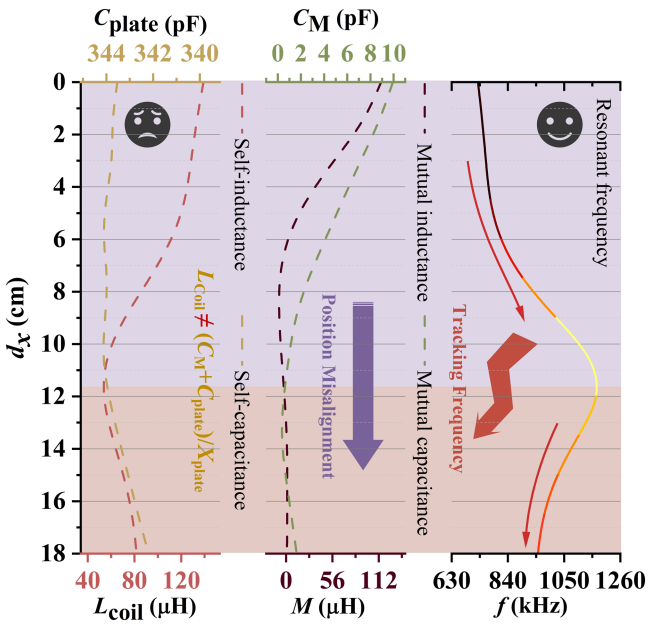

Fig. 7. Coupled power transfer method based on tracking frequency.

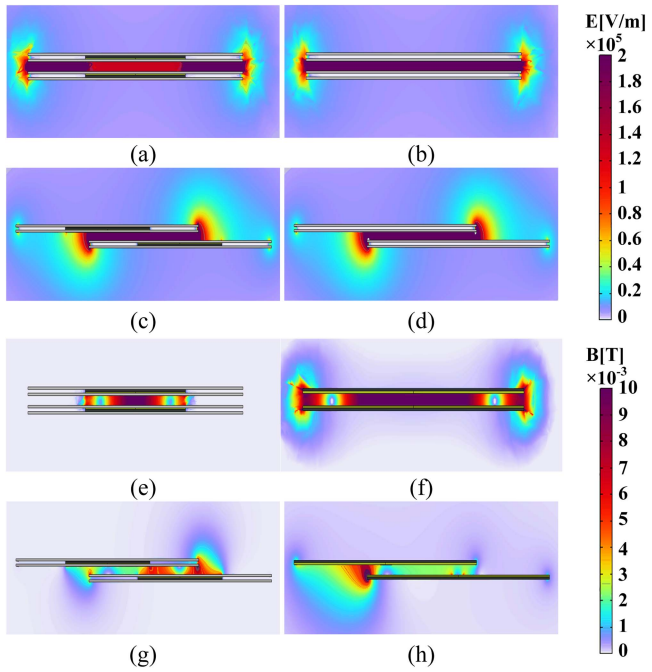

Fig. 8. EMF distribution around the couplers of different types of WPT systems in the aligned and misalignment states. (a) Electric field (HWPT-not misalignment). (b) Electric field (CPT-not misalignment). (c) Electric field (HWPT-misalignment 120 mm). (d) Electric field (CPT-misalignment 120 mm). (e) Magnetic flux (HWPT-not misalignment). (f) Magnetic flux (IPT-not misalignment). (g) Magnetic flux (HWPT-misalignment 120 mm). (h) Magnetic flux (IPT-misalignment 120 mm).

Fig. 8 shows the EMF distribution around the couplers of different types of WPT systems in the aligned and misalignment states. The HWPT's integrated coupler is sized as in the setup

of Figs. 6 and 7. The CPT's coupler consists of vertically placed metal plates with the length of 300 mm, separated by the gap of 2 mm. The IPT's coupler consists of a 1 mm wire radius coil with 70 turns and 10 mm inner diameter. The coil is covered with a ferrite on the backside, and the x- and y-axis dimensions of the ferrite match the coil.

Fig. 8(a), (c), (e), and (g) shows the EMF distribution around the HWPT's integrated coupler. From Fig. 8(a) and (e), most of the aligned case's electric field and magnetic flux are effectively confined within the HWPT's integrated coupler. Specifically, the electric field distribution is similar in both cases compared to the CPT's coupler [see Fig. 8(b)]. Compared to the IPT's coupler [see Fig. 8(f)], the electromagnetic safety of the integrated coupler is improved due to the electric shielding effect of the aluminum metal plates. When the integrated coupler undergoes positional misalignment, the electric field and magnetic flux increase in the unaligned area, as shown in Fig. 8(c) and (g). This is the primary reason for the deterioration of the output characteristics of the system. The electric field distribution of the integrated coupler in the misalignment state is similar to that of the CPT's coupler [see Fig. 8(d)]. Meanwhile, compared to the IPT's coupler [see Fig. 8(h)], the electromagnetic safety of the integrated coupler in the misalignment state is improved due to the reduced level of electromagnetic exposure.

Through the integrated coupler and the coupled power transfer method based on frequency tracking proposed in this article, the HWPT system can realize the synergistic transfer of two types of coupled powers under any position misalignment. The simulation results demonstrate that the proposed coupled power transfer method can ensure the system is in the optimal resonant state, even in position misalignment. Meanwhile, the proposed integrated coupler enhances the electromagnetic safety of the system compared with the single-type coupler.

IV. Experiment

A. Experimental Platform

An experimental platform is built to validate the proposed HWPT system, shown in Fig. 9. Table II compares the design values (consistent with Section III-C) with the measured values. The experimental platform's input power is 500 W. The coils are made of 220-strand Litz wire. The diameter of Litz wire strands is 0.13 mm. Considering that the skin depth of copper is 65.2 μm at 1 MHz, there is no significant increase in ac resistance due to the skin effect. The transmitting and receiving coil resistances are 1.13 Ω and 1.02 Ω, respectively. The magnetic shielding is TDK PC95 type ferrite with 2 mm thickness. The thickness of the metal plates is 2 mm.

The integrated coupler proposed in this article consists of the coil and the capacitor, which needs extra attention for the insulation of the coupler. The ferrite is used to widen the distance between the coil and the metal plate, while the part of the metal plate close to the coil is coated with high-voltage insulating tape to avoid the breakdown between the coil and the metal plate. To avoid breakdowns between the plates, the distance between the plates is widened using the insulating shims. The air is a great insulating medium. The breakdown voltage of dry air is 3.0 kV/mm, and t_m is 2 mm, so there is no concern with arcing.

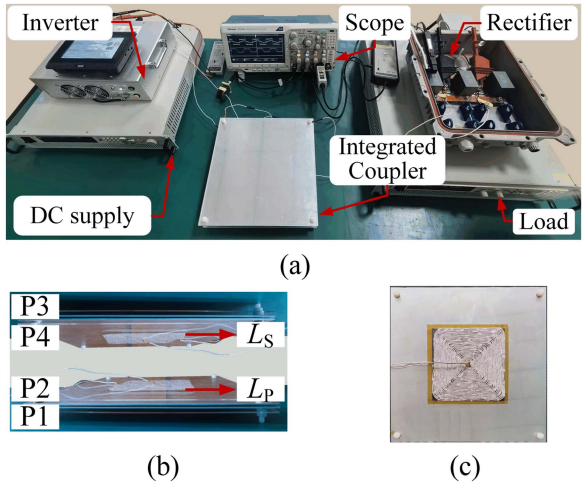

Fig. 9. Experimental platform of the HWPT system. (a) Experimental platform. (b) Longitudinal section. (c) Integrated coupler.

TABLE II
Experimental Parameters

Parameter	Design value	Measurement
l_b	300 mm	300 mm
r	1 mm	1 mm
d_c	10 mm	10 mm
w_P	80 mm	80 mm
t_m	2 mm	2 mm
d	10 mm	10 mm
N	30	30
P_{IN}	500 W	500 W
R_L	40 Ω	40 Ω
L_P	139 μH	130 μH
L_S	139 μH	141 μH
C_1	344 pF	334 pF
C_2	344 pF	350 pF
M (not misalignment)	115 μH	117 μH
M (d_x = 120 mm)	1.45 μH	1.55 μH
C_M (not misalignment)	9.93 pF	10.3 pF
C_M (d_x = 120 mm)	1.16 pF	1.22 pF

Fig. 10 shows the change in the integrated coupler's inductance and capacitance when the position of the integrated coupler is misaligned. Both mutual inductance and mutual capacitance decrease, which is the main reason for the decrease in the system efficiency of the single coupling system. To overcome this problem, this article improves the power transfer capability of the system in the misaligned state by introducing two types of coupled powers. Compared with the IPT system, the essence proposed in this article is the introduction of mutual capacitance to compensate for the excess leakage flux in the misaligned state. Compared with the CPT system, the essence of the system proposed in this article is the introduction of mutual inductance to enhance the coupling coefficient of the EMF. In addition, as shown in Fig. 10, it is evident that the actual measured values are in close agreement with the simulation results of Section III-C.

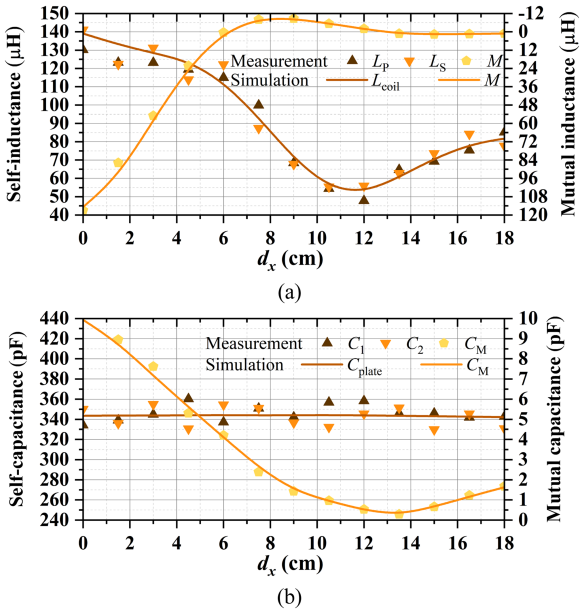

Fig. 10. Comparison of simulation and measurement results. (a) Inductance. (b) Capacitance.

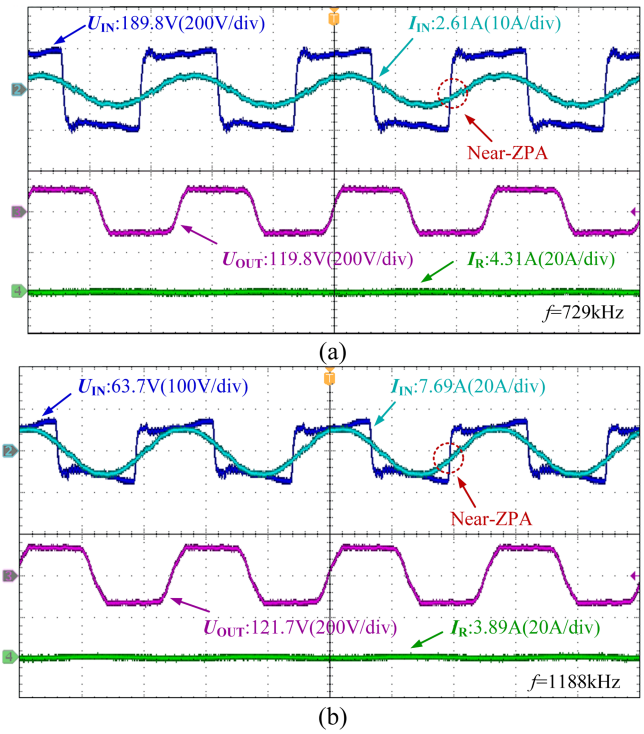

Fig. 11. Experimental waveforms of the inverter and load. (a) no misalignment. (b) $d_x = 120$ mm.

Fig. 11(a) shows the voltage and current waveforms of the system when the position of the integrated coupler is not misaligned and the system satisfies the near-ZPA input. The system's received power is 438 W, and the system efficiency from ac to ac is 88.5%. The coupled power transmitted through the magnetic field is calculated in (10) as 422 W, and the coupled power transmitted through the electric field is calculated in (11) as

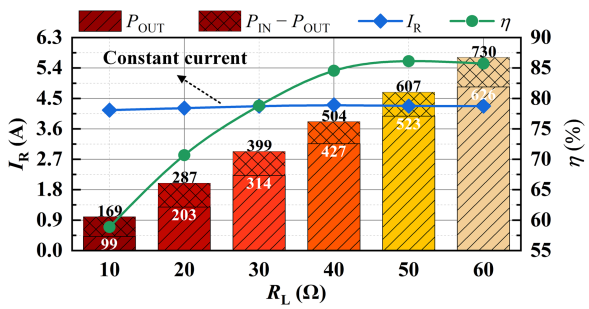

Fig. 12. Measured load current, power, and efficiency under different loads.

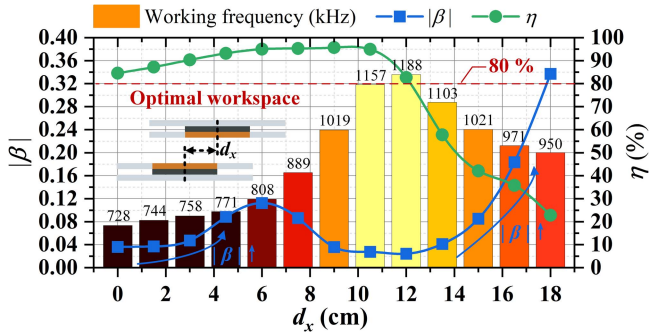

Fig. 13. Measured working frequency, efficiency, and power ratio under unidirectional misalignment.

16 W. Fig. 11(b) shows the system's voltage and current waveforms when the integrated coupler's position is unidirectional misaligned 120 mm. The system's working frequency is changed from 728 to 1188 kHz. By adjusting the working frequency, the system resonance is restored, and the system satisfies the near-ZPA input. The system's received power is 413 W. The system efficiency from ac to ac is 84.2%. The coupled power transmitted through the magnetic field and the electric field is 403 W and 10 W, respectively. The HWPT system can realize the synergistic transfer of the two types of coupled powers.

B. Experimental Validation of the CC

Fig. 12 shows the variation of the load current, system efficiency (dc–dc), and transfer power with dc load. The load current is independent of the dc load, and its value remains around 4.3 A. It indicates that the HWPT system proposed in this article has the CC output characteristics. The system efficiency is not less than 85% when the dc load is 40–60 Ω. When $R_L = 50$ Ω, the system's input power is 607 W, the system efficiency is 86.2%, and the system loss power is 84 W.

C. Experimental Validation of the Misalignment Tolerance

Fig. 13 shows the variations of working frequency, system efficiency (dc to dc), and the ratio of two types of coupled powers when the position of the integrated coupler is unidirectionally misaligned. The HWPT system achieves the resonance state (near ZPA input) at any position misalignment through the coupled power transfer method based on frequency tracking. When

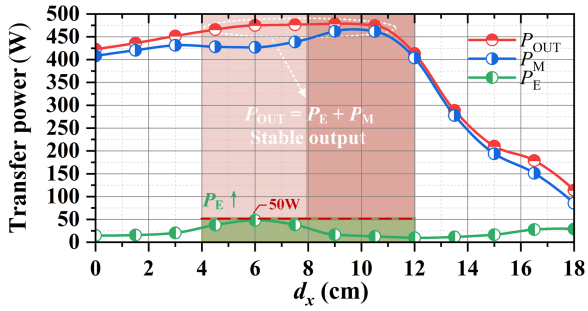

Fig. 14. Measured output power and the two types of coupled powers unidirectional misalignment.

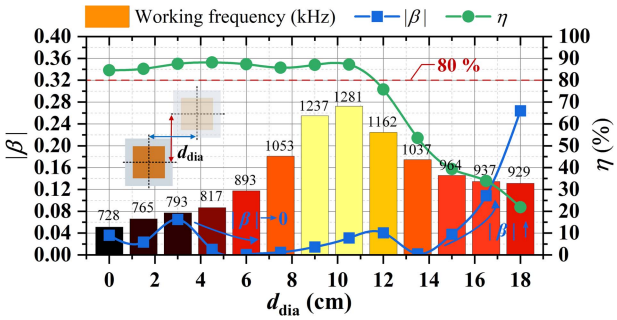

Fig. 15. Measured working frequency, efficiency, and power ratio under diagonal misalignment.

the displacement of the integrated coupler is less than 120 mm, the system efficiency from dc to dc remains relatively high at over 80% and reaches up to 95.7% ($d_x = 90$ mm). Simultaneously, the ratio of two types of coupled powers exhibits an initial increase, followed by a decrease, and then another increase. When the displacement of the integrated coupler is 60 mm, this ratio reaches its first peak (0.11). This ratio rises rapidly when the displacement of the integrated coupler exceeds 120 mm, and the rate of the rise is larger than when the displacement is less than 60 mm. The coupler's maximum unidirectional misalignment distance is defined as the unidirectional misalignment distance when the system efficiency is at least 80%. The HWPT system proposed in this article has a higher unidirectional misalignment tolerance and its maximum unidirectional misalignment distance is 120 mm.

Fig. 14 shows the variations of the output power and the two types of coupled powers when the position of the integrated coupler is unidirectionally misaligned. The coupled power transmitted through the electric field (P_E) increases when d_x<60 mm. Especially when $d_x = 60$ mm, P_E reaches a maximum value of 47.4 W. When 0<d_x<60 mm, the HWPT system's unidirectional misalignment tolerance is enhanced due to the introduction of P_E. The P_E decreases when d_x>60 mm. However, the HWPT system's output power (P_{OUT}) is still stable for 60 mm< d_x<120 mm. This is due to increased coupled power transmitted through the magnetic field (P_M). The output characteristics of the HWPT system are similar to that of the IPT system with SS-type compensation topology when k_E enters the weak coupling region. The magnetic field coupled power increases within a certain range when k_M enters the weak coupling range, and the system efficiency of IPT decreases. However, the system efficiency of the HWPT system proposed in this article has increased, mainly due to the introduction of $P_{E,}$ which is still considerable. Due to the complementary effects of P_M and P_E within the range of unidirectional misalignment from 40 to 120 mm, the HWPT system achieves stable power output.

The integrated coupler proposed in this article is not strictly axisymmetric. To analyze the complete misalignment characteristics of the HWPT system proposed in this article, the output characteristics of the HWPT system are analyzed under diagonal misalignment. d_{dia} denotes the diagonal misalignment and satisfies $d_{dia} = d_x = d_y$. Fig. 15 shows the variations of working frequency, system efficiency (dc to dc), and the

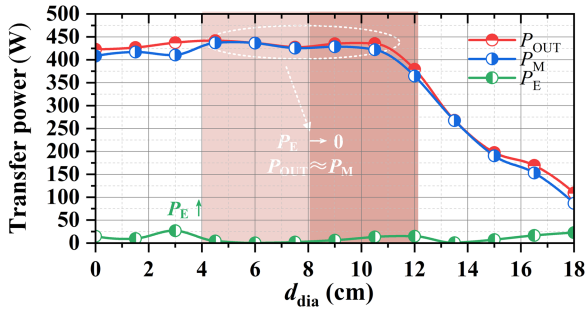

Fig. 16. Measured output power and the two types of coupled powers diagonally misalignment.

ratio of two types of coupled powers when the position of the integrated coupler is diagonally misaligned. Similar to the system characteristics under unidirectional misalignment, the system efficiency (dc to dc) remains high at over 80% when the diagonal displacement of the integrated coupler is less than 110 mm. However, the overall system efficiency declines with the diagonal misalignment. Meanwhile, the ratio of two types of coupled powers shows an increasing, decreasing, increasing, decreasing, increasing trend. When the diagonal displacement of the integrated coupler is 30 mm, this ratio reaches its first peak (0.065). This ratio rises rapidly when the diagonal displacement of the integrated coupler exceeds 130 mm. The output characteristics of the HWPT system proposed in this article do not meet the expectations when the coupler is diagonally misaligned. Although the system remains at a high level of transmission efficiency, the transmission efficiency continues to decline through the diagonal misalignment process.

Fig. 16 shows the variations of the output power and the two types of coupled powers when the position of the integrated coupler is diagonally misaligned. Similar to the system characteristics under unidirectional misalignment, the coupled power transmitted through the electric field (P_E) increases when d_{dia}<30 mm. Especially when $d_{dia} = 30$ mm, P_E reaches a maximum value of 26.7 W. When 0<d_{dia}<30 mm, the HWPT system's misalignment tolerance is enhanced due to the introduction of P_E. The P_E decreases when d_{dia}>30 mm. The overall output power (P_{OUT}) of the HWPT system decreases with the diagonal misalignment due to the introduction of the P_E is not considerable. At this point, P_{OUT} is approximately equal

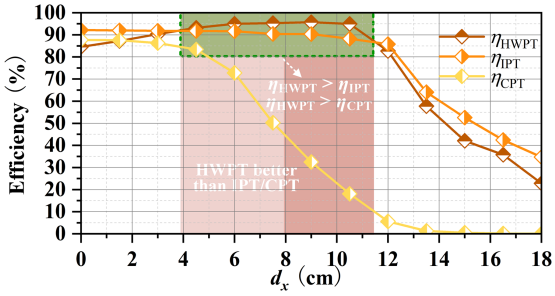

Fig. 17. Experimental results of efficiency in the hybrid system and single coupling system.

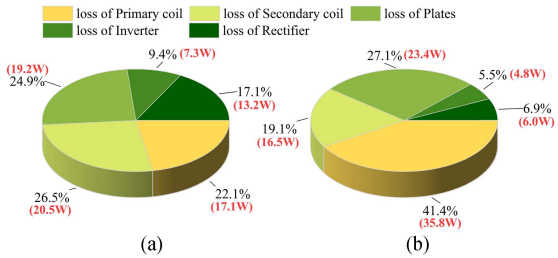

Fig. 18. Estimated power losses distribution of the experimental system. (a) No misalignment. (b) $d_x = 120$ mm.

to P_M. Unlike the system characteristics under unidirectional misalignment, it should be noted that the magnetic field coupled power of the HWPT system does not increase when k_E enters the weak coupling region. It is due to the increase of the coil losses when the diagonal misalignment is affected by the integrated coupler's structure. According to Figs. 15 and 16, the diagonal misalignment tolerance of the HWPT system proposed in this article does not meet the expectations. The main reason for this phenomenon is the integrated coupler's structure. When the coupler is diagonally misaligned, the system's coil losses increase, but the electric field coupled power provided by the metal plates is not considerable.

Based on the discussion in this part, the HWPT system proposed in this article has strong unidirectional misalignment tolerance, but its diagonal misalignment tolerance could be better. Based on the analyses of the system misalignment characteristics and transmission efficiency in Sections II-B and C, further optimization of the integrated coupler's structure is required to achieve a higher degree of freedom of misalignment tolerance.

D. Comparison of HWPT With Single IPT and CPT System

According to the discussion in Section II-B, the system's initial resonance state is disrupted by changes in the integrated coupler's electrical parameters when the position of the integrated coupler is misaligned. To realize the HWPT with high misalignment tolerance characteristics, Section III-A proposes a transfer method to compensate for the change in the integrated coupler's electrical parameters owing to misalignment by adjusting the system's working frequency. To validate the proposed HWPT system's misalignment tolerance, it is compared with the IPT system and the CPT system under the same conditions. These conditions include coupler size, transmission distance and misalignment. Fig. 17 shows the variation of the system efficiencies of the three different types of transfer systems when the position of the coupler is unidirectionally misaligned. It should be noted that the above-mentioned efficiencies are all transmission efficiencies from the dc source to the rectifier (dc–dc), and they are obtained by measuring the active power flowing into the load and the active power flowing into the system from the dc source by using the oscilloscope and calculating the ratios. Comparing the output characteristics of three types of WPT systems using the couplers of the same size and all with 10 mm transmission distance. The IPT's coupler and the CPT's coupler have the same size as those shown in Fig. 8 in Section III-C. To ensure the validity of the comparison experiment, the IPT system and the CPT system are fully compensated at any positional misalignment by adjusting the system working frequency.

With the displacement of the coupler, the system efficiency decreases for both the IPT and the CPT systems. Within the range of unidirectional misalignment from 40 to 110 mm, the HWPT system's efficiency exceeds that of the IPT system and the CPT system. The HWPT system exhibits strong tolerance to unidirectional misalignment through the synergistic transfer of the two types of coupled powers. The maximum unidirectional misalignment distance for the proposed HWPT system and IPT system under the same conditions are both 120 mm. When $40 < d_x < 110$ mm, the system efficiency of the proposed HWPT system is better than that of the IPT system under the same conditions. The maximum unidirectional misalignment distance for the CPT system and the proposed HWPT system under the same conditions are 50 mm and 120 mm, respectively. Compared with the CPT system, the unidirectional misalignment tolerance of the proposed HWPT system is improved by 140%.

E. Loss Analysis

Fig. 18(a) and (b) shows the distribution of the system losses among the circuit components when the position of the integrated coupler is not misaligned and $d_x = 120$ mm, respectively. The data for the analysis are based on experimental measurement and calculation. The system power losses come from switching devices' switching transitions, diodes' conduction, and the integrated coupler's losses. Specifically, most of the power losses are dissipated in the integrated coupler due to its low-quality factor. In addition to the ac losses in the coil, the magnetic field generated by the coil produces additional eddy current losses in the aluminum metal plate. The integrated coupler's hybrid coupling coefficient and quality factor will be improved in future designs to widen the coupled power transmission channel.

This article proposes an integrated coupler consisting of a coil and a capacitor (metal plate) to realize the synergistic transfer of the two types of coupled power. The metal plate can be viewed as a foreign object, increasing the losses for the coil. The additional losses increase with system unidirectional misalignment since part of the metal plates moves into the center of the coil. The losses of the primary coil increase under unidirectional misalignment, as shown in Fig. 14. However, the proposed HWPT system's efficiency increases with the unidirectional misalignment because the metal plate intervening in the coils' magnetic field not only increases the system losses

TABLE III
COMPARISON OF RECENT SYSTEMS ON THIS TOPIC

Items	Frequency	Coupler	Compensation topology	Maximum unidirectional misalignment ratio	Efficiency	ZPA	CC/CV
[12]	1 MHz	Heavy	Double-sided LC	x-misalignments: 22% y-misalignments: 22%	94.5% (aligned)	Yes	CC
[13]	1 MHz	Heavy	Double-sided LCL	N/A	73.6% (aligned)	Yes	CC
[14]	800 kHz	Heavy	SS	N/A	91.9% (aligned)	Yes	CC
[15]	1 MHz	Light	Double-sided LC	x-misalignments: 45% y-misalignments: 45%	85.8% (aligned)	Yes	CC
[19]	2.5 MHz	Light	Double-sided LC	x-misalignments: 10% y-misalignments: 13%	85.7% (misalignment 10%)	NO	CC
[20]	6.78 MHz	Light	No compensation components	x-misalignments: 33% y-misalignments: 33%	81.4% (aligned)	Yes	CC
[21]	1 MHz	Light	Double-sided LC	x-misalignments: 25% y-misalignments: 25%	86.5% (misalignment 30%)	Yes	CC
This work	728−1188 kHz	Light	No compensation components	x-misalignments: 40% y-misalignments: 40%	95.7% (misalignment 30%)	Yes	CC

but also acts the carrier to transfer the electric field coupled power. The two types of effects have opposite contributions to the system efficiency. Whether the unidirectional misalignment characteristics of the HWPT system proposed in this article are improved or worsened is the result of the game of the two types of effects. Simulation and experimental results show that the coupler, which introduces metal plates, improves the unidirectional misalignment characteristics of the WPT system. The reasons for this are analyzed as follows.

1) The area of the metal plates (P2&P4) close to the coil is limited, so the generating additional losses are limited. The metal plates with the bigger area (P1&P3) are far away from the coil, and the ferrite binds the magnetic field generated by the coil, so additional losses are also limited.
2) The metal plate can serve as the carrier of the electric field coupling transmission channel and compensate for the decrease in the coupled power transmitted through the magnetic field due to unidirectional misalignment.

For the abovementioned reasons, the increase of system losses by the introduction of the metal plate is limited; the increased system losses from the introduction of the metal plate are limited, but the electric field coupled power it provides is considerable. So, the output characteristics of the WPT system are improved (unidirectional misalignment tolerance is enhanced).

F. Comparison and Discussion

To highlight the superiority of the HWPT system proposed in this article, a comprehensive comparison of it with other HWPT systems is presented in Table III. Meanwhile, define d_x/l_b as the system's unidirectional misalignment ratio. The HWPT system proposed in this article can achieve 82.7% system efficiency from dc to dc at 40% unidirectional misalignment.

The maximum unidirectional misalignment ratio is the ratio of the integrated coupler's maximum displacement to the coupler's length. In particular, the coupler's length is defined as the sum of the lengths of the coil and the metal plate in some HWPT systems where the coupler is separated. Upon reviewing the table, the HWPT system proposed in this article has high integration and unidirectional misalignment tolerance. The proposed system integrates all the compensation components into the coupler compared with the coupler in [12], [13], and [14], reducing the system size. Compared with [12], [13], [14], [15], [19], and [21], the proposed system achieves no compensation components in the main circuit by relying on the integrated coupler, which enhances the integration of the system. The proposed transfer method provides better dc–dc efficiency compared with [13], [15], [19], [20], and [21]. Moreover, in addition to [15], the proposed system offers relatively better unidirectional misalignment tolerance CC output than the existing HWPT systems.

The major differences between the HWPT system proposed in this article and the existing work are as follows.

1) It is a self-resonant system in the whole sense, and there is no additional compensation component.
2) Attention is paid to the problem of resonance point drift during unidirectional misalignment, and frequency tracking ensures that the system is in the best state.

The work in this article will inform the further development of HWPT and perfect the HWPT technique in terms of unidirectional misalignment.

V. CONCLUSION

This article proposes a new HWPT system with a novel integrated coupler based on tracking frequency. The coupler is integrated into the system's main circuit to realize no extra compensation components. Through the synergistic transfer of two types of coupled powers with complementary characteristics, the system has a higher unidirectional misalignment tolerance than the conventional single coupling system. The following conclusions are obtained.

For the proposed integrated coupler, the capacitor and coil overlap in a coaxial arrangement, and its electrical parameters are influenced by the spatial structure of the two types of materials under the limited axial projection area. According to the proposed power transfer method for the HWPT system, the resonance state is maintained by frequency tracking, and the system realizes the synergistic transfer of the coupled power transmitted through the magnetic field and the coupled power transmitted through the electric field. Due to the complementary

output of the two types of coupled powers, the proposed HWPT system has a higher unidirectional misalignment tolerance. A 500-W HWPT experimental platform is built to validate the transfer method's effectiveness and achieve 82.7% system efficiency from dc to dc at 40% unidirectional misalignment.

REFERENCES

[1] Z. Zhang, H. Pang, A. Georgiadis, and C. Cecati, "Wireless power transfer-an overview," *IEEE Trans. Ind. Electron.*, vol. 66, no. 2, pp. 1044–1058, Feb. 2019.

[2] J. Lian and X. Qu, "An LCLC-LC-compensated capacitive power transferred battery charger with near-unity power factor and configurable charging profile," *IEEE Trans. Ind. Appl.*, vol. 58, no. 1, pp. 1053–1060, Jan./Feb. 2022.

[3] C. Cheng, T. Chen, X. Cui, Y. Liu, S. Zhang, and C. Mi, "Harmonic modeling and analysis of series-parallel compensated IPT systems with an inductive filter," *IEEE Trans. Power Electron.*, vol. 38, no. 11, pp. 13405–13414, Aug. 2023.

[4] W. Zhou, L. Huang, B. Luo, R. Mai, Z. He, and A. P. Hu, "A general mutual coupling model of MIMO capacitive coupling interface with arbitrary number of ports," *IEEE Trans. Power Electron.*, vol. 36, no. 6, pp. 6163–6167, Jun. 2021.

[5] T. Chen, C. Cheng, H. Cheng, C. Wang, and C. C. Mi, "Load-independent power-repeater capacitive power transfer system with multiple constant voltage outputs," *IEEE J. Emerg. Sel. Top. Power Electron.*, vol. 10, no. 5, pp. 6358–6370, Oct. 2022.

[6] T. Chen, C. Cheng, H. Cheng, C. Wang, and C. C. Mi, "A multi-load capacitive power relay system with load-independent constant current outputs," *IEEE Trans. Power Electron.*, vol. 37, no. 5, pp. 6144–6155, May 2022.

[7] J. Kim, K. Kim, H. Kim, D. Kim, J. Park, and S. Ahn, "An efficient modeling for underwater wireless power transfer using Z-parameters," *IEEE Trans. Electromagn. Compat.*, vol. 61, no. 6, pp. 2006–2014, Dec. 2019.

[8] F. Wang, Q. Yang, X. Zhang, Z. Yuan, and X. Ni, "Optimizing levitation devices for wireless power transfer: An Fe-NCS grid structure approach," *IEEE Trans. Power Electron.*, vol. 38, no. 10, pp. 11859–11869, Oct. 2023.

[9] X. Zhang, X. Ma, Z. Yuan, F. Xu, Z. Chen, and F. Wang, "Misalignment-tolerant integration for S- LCC -compensated WPT systems: A complementary-coupling compact receiver," *IEEE Trans. Power Electron.*, vol. 38, no. 10, pp. 11907–11915, Oct. 2023.

[10] J. Dai and D. C. Ludois, "A survey of wireless power transfer and a critical comparison of inductive and capacitive coupling for small gap applications," *IEEE Trans. Power Electron.*, vol. 30, no. 11, pp. 6017–6029, Nov. 2015.

[11] X. Gao et al., "Design and analysis of a new hybrid wireless power transfer system with a space-saving coupler structure," *IEEE Trans. Power Electron.*, vol. 36, no. 5, pp. 5069–5081, May 2021.

[12] F. Lu, H. Zhang, H. Hofmann, and C. C. Mi, "An inductive and capacitive combined wireless power transfer system with LC -compensated topology," *IEEE Trans. Power Electron.*, vol. 31, no. 12, pp. 8471–8482, Dec. 2016.

[13] F. Lu, H. Zhang, H. Hofmann, and C. C. Mi, "An inductive and capacitive integrated coupler and its LCL compensation circuit design for wireless power transfer," *IEEE Trans. Ind. Appl.*, vol. 53, no. 5, pp. 4903–4913, Sep./Oct. 2017.

[14] B. Luo, T. Long, R. Mai, R. Dai, Z. He, and W. Li, "Analysis and design of hybrid inductive and capacitive wireless power transfer for high-power applications," *IET Power Electron*, vol. 11, no. 14, pp. 2263–2270, 2018.

[15] B. Luo, T. Long, L. Guo, R. Dai, R. Mai, and Z. He, "Analysis and design of inductive and capacitive hybrid wireless power transfer system for railway application," *IEEE Trans. Ind. Appl.*, vol. 56, no. 3, pp. 3034–3042, May/Jun. 2020.

[16] Z. Yuan, M. Saeedifard, C. Cai, Q. Yang, P. Zhang, and H. Lin, "A misalignment tolerant design for a dual-coupled LCC -S-compensated WPT system with load-independent CC output," *IEEE Trans. Power Electron.*, vol. 37, no. 6, pp. 7480–7492, 2022.

[17] Z. Dai and J. Wang, "A dual-frequency WPT based on multilayer self-decoupled compact coil and dual CLCL hybrid compensation topology," *IEEE Trans. Power Electron.*, vol. 37, no. 11, pp. 13955–13965, Nov. 2022.

[18] X. Y. Zhang, C. Xue, and J. Lin, "Distance-insensitive wireless power transfer using mixed electric and magnetic coupling for frequency splitting suppression," *IEEE Trans. Microw. Theory Tech.*, vol. 65, no. 11, pp. 4307–4316, Nov. 2017.

[19] J. Zhu, Y. Ban, R. Xu, and C. C. Mi, "An NFC-connected coupler using IPT-CPT-combined wireless charging for metal-cover smartphone applications," *IEEE Trans. Power Electron.*, vol. 36, no. 6, pp. 6323–6338, Jun. 2021.

[20] X. Chen, S. Yu, and Z. Zhang, "A receiver-controlled coupler for multiple output wireless power transfer applications," *IEEE Trans. Circuits Syst. I Reg. Paper*, vol. 66, no. 11, pp. 4542–4552, Nov. 2019.

[21] X. Qing, Z. Li, X. Wu, Z. Liu, L. Zhao, and Y. Su, "A hybrid wireless power transfer system with constant and enhanced current output against load variation and coupling misalignment," *IEEE Trans. Power Electron.*, vol. 38, no. 10, pp. 13219–13230, Oct. 2023.

[22] H. Zhang, F. Lu, H. Hofmann, W. Liu, and C. C. Mi, "A four-plate compact capacitive coupler design and LCL -compensated topology for capacitive power transfer in electric vehicle charging application," *IEEE Trans. Power Electron.*, vol. 31, no. 12, pp. 8541–8551, Dec. 2016.

Fengxian Wang received the B.S. degree in electrical engineering and the M.S. degree in electrical engineering from Tiangong University, Tianjin, China, in 2018 and 2021, respectively. He is currently working toward the Ph.D. degree in electrical engineering from the Hebei University of Technology, Tianjin, China.

His research interests include engineering electromagnetism, wireless power transfer, and its industrial applications.

Qingxin Yang received the B.S., M.S., and Ph.D. degrees in electrical engineering from the Hebei University of Technology, Tianjin, China, in1983, 1986, and 1997, respectively.

Since 1996, he has been a Professor with the Hebei University of Technology. From 2008 to 2018, he was the President of Tianjin Polytechnic University, Tianjin, China. From 2018 to 2020, he was the President of the Tianjin University of Technology, Tianjin, China. His research interests include computational electromagnetism, engineering electromagnetism and their applications, and special wireless power transfer.

Dr. Yang was a Board Member of International COMPUMAG Society and the President of China chapter. Since 2015, he has been the President of China Electrotechnical Society.

Xian Zhang received the M.E. and Ph.D. degrees in electrical engineering from the Hebei University of Technology, Tianjin, China, in 2009 and 2012, respectively.

He is currently a Professor with the Hebei University of Technology, Tianjin, China. He is the Director of the China Electrotechnical Society and the Secretary-General of the National Specialized Committee on Wireless Power Transmission Technology. His research interests include intelligent high-power wireless power transmission technology, measurement of three-dimensional electromagnetic fields, and numerical calculations of modern engineering electromagnetic fields.

Ting Chen (Member) received the B.S., M.S., and Ph.D. degrees in electrical engineering from the China University of Mining and Technology, Beijing, China, in 2015, 2017, and 2022, respectively.

From 2019 to 2021, she was a joint Ph.D. student with the Department of Electrical and Computer Engineering, San Diego State University, San Diego, CA, USA. She is currently with the Department of Electrical Engineering and State Key Laboratory of Reliability and Intelligence of Electrical Equipment, Hebei University of Technology. Her current research interests include wireless power transfer technologies, and modeling and control of switching converters.

Guangyao Li received the B.S. degree in electrical engineering and intelligent control from the Tianjin Sino-German University of Applied Sciences, Tianjin, China, in 2022. He is currently working toward the M.E. degree in electrical engineering with the Hebei University of Technology, Tianjin, China.

His research interests include engineering electromagnetism, wireless power transfer, and its industrial applications.